Bendable, low-loss Topas fibers for the terahertz frequency range

Nielsen, Kristian; Rasmussen, Henrik K.; Adam, Aurèle J.L.; Planken, Paul C M.; Bang, Ole; Jepsen, Peter Uhd

Published in:
Optics Express

Link to article, DOI:
10.1364/OE.17.008592

Publication date:
2009

Document Version
Publisher's PDF, also known as Version of record

Bendable, low-loss Topas fibers for the terahertz frequency range

Kristian Nielsen[1], Henrik K. Rasmussen[2], Aurèle J. L. Adam[3], Paul C. M. Planken[3], Ole Bang[1], and Peter Uhd Jepsen[1]

[1]*Technical University of Denmark, DTU Fotonik - Department of Photonics Engineering, DK-2800 Kongens Lyngby, Denmark*
[2]*Technical University of Denmark, Department of Mechanical Engineering, DK-2800 Kongens Lyngby, Denmark*
[3]*Delft University of Technology, Faculty of Applied Sciences, Department of Imaging Science and Technology, Lorentzweg 1, 2628 CJ Delft, the Netherlands*

puje@fotonik.dtu.dk

Abstract: We report on a new class of polymer photonic crystal fibers for low-loss guidance of THz radiation. The use of the cyclic olefin copolymer Topas, in combination with advanced fabrication technology, results in bendable THz fibers with unprecedented low loss and low material dispersion in the THz regime. We demonstrate experimentally how the dispersion may be engineered by fabricating both high- and low-dispersion fibers with zero-dispersion frequency in the regime 0.5-0.6 THz. Near-field, frequency-resolved characterization with high spatial resolution of the amplitude and phase of the modal structure proves that the fiber is single-moded over a wide frequency range, and we see the onset of higher-order modes at high frequencies as well as indication of microporous guiding at low frequencies and high porosity of the fiber. Transmission spectroscopy demonstrates low-loss propagation ($<$ 0.1 dB/cm loss at 0.6 THz) over a wide frequency range.

OCIS codes: (300.6495) Spectroscopy, terahertz; (180.4243) Near-field microscopy; (060.2280) Fiber design and fabrication; (060.2270) Fiber characterization

References and links

1. M. Tonouchi, "Cutting-edge teraherz technology," Nat. Photon. **1,** 97–105 (2007)
2. Y. He, P. I. Ku, J. R. Knab, J. Y. Chen, and A. G. Markelz, "Protein dynamical transition does not require protein structure," Phys. Rev. Lett. **101,** 178103 (2008)
3. C. Kübler, H. Ehrke, R. Huber, R. Lopez, A. Halabica, R. F. Haglund, Jr., and A. Leitenstorfer, "Coherent structural dynamics and electronic correlations during an ultrafast insulator-to-metal phase transition in VO_2," Phys. Rev. Lett. **99,** 116401 (2007)
4. A. J. L. Adam, J. M. Brok, M. A. Seo, K. J. Ahn, D. S. Kim, J. H. Kang, Q. H. Park, M. Nagel, and P. C. M. Planken, "Advanced terahertz electric near-field measurements at sub-wavelength diameter metallic apertures," Opt. Express **16,** 7407–7417 (2008)
5. T. A. Birks, J. C. Knight, and P. St. J. Russell, "Endlessly single-mode photonic crystal fiber," Opt. Lett. **22,** 961–963 (1997)
6. A. Hassani, A. Dupuis, and M. Skorobogatiy, "Low loss porous terahertz fibers containing multiple subwavelength holes," Appl. Phys. Lett. **92,** 071101 (2008)
7. A. Hassani, A. Dupuis, and M. Skorobogatiy, "Porous polymer fibers for low-loss terahertz guiding," Opt. Express **16,** 6340–6351 (2008)
8. S. Atakaramians, S. Afshar V., B. M. Fischer, D. Abbott, and T. M. Monro, "Porous fibers: a novel approach to low loss THz waveguides," Opt. Express **16,** 8845–8854 (2008)

#108854 - $15.00 USD Received 16 Mar 2009; revised 4 May 2009; accepted 4 May 2009; published 6 May 2009

9. S. Atakaramians, S. Afshar V., B. M. Fischer, D. Abbott, and T. M. Monro, "Low loss, low dispersion and highly birefringent terahertz porous fibers," Opt. Commun. **282,** 36–38 (2009)
10. G. Gallot, S. P. Jamison, R. W. McGowan, and D. Grischkowsky, "Terahertz waveguides," J. Opt. Soc. Am. B **17,** 851–863 (2000)
11. R. Mendis and D. Grischkowsky, "Plastic ribbon THz waveguides," J. Appl. Phys. **88,** 4449–4451 (2000)
12. R. Mendis and D. Grischkowsky, "Undistorted guided-wave propagation of subpicosecond terahertz pulses," Opt. Lett. **26,** 846–848 (2001)
13. R. Mendis and D. Grischkowsky, "THz interconnect with low-loss and low-group velocity dispersion," IEEE Microw. Wirel. Compon. Lett. **11,** 444–446 (2001)
14. K. Wang and D. M. Mittleman, "Metal wires for terahertz wave guiding," Nature **432,** 376–379 (2004)
15. L.-J. Chen, H.-W. Chen, T.-F. Kao, J.-Y. Lu, and C.-K. Sun, "Low-loss subwavelength plastic fiber for terahertz waveguiding," Opt. Lett. **31,** 308–310 (2006)
16. B. Bowden, J. A. Harrington, and O. Mitrofanov, "Silver/polystyrene-coated hollow glass waveguides for the transmission of terahertz radiation," Opt. Lett. **32,** 2945–2947 (2007)
17. H. Han, H. Park, M. Cho, and J. Kim, "Terahertz pulse propagation in a plastic photonic crystal fiber," Appl. Phys. Lett. **80,** 2634–2636 (2002)
18. M. Goto, A. Quema, H. Takahashi, S. Ono, and N. Sarukura, "Teflon photonic crystal fiber as terahertz waveguide," Jpn. J. Appl. Phys. **43,** L317–L319 (2004)
19. M.A. van Eijkelenborg, M.C.J. Large, A. Argyros, J. Zagari, S. Manos, N.A. Issa, I. Bassett, S. Fleming, R.C. McPhedran, C.Martijn de Sterke, and N.A.P. Nicorovici, "Microstructured polymer optical fibre," Opt. Express **9**, 319-327 (2001).
20. C. S. Ponseca, Jr., R. Pobre, E. Estacio, N. Sarukura, A. Argyros, M. C. J. Large, and M. A. can Eijkelenberg, "Transmission of terahertz radiation using a microstructured polymer optical fiber," Opt. Lett. **33,** 902–904 (2008)
21. Y. F. Geng, X. L. Tan, P. Wang, and J. Q. Yao, "Transmission loss and dispersion in plastic terahertz photonic band-gap fibers," Appl. Phys. B **91,** 333–336 (2008)
22. G. Emiliyanov, J. B. Jensen, O. Bang, P. E. Hoiby, L. H. Pedersen, E. Kjær, and L. Lindvold, "Localized biosensing with Topas microstructured polymer optical fiber," Opt. Lett. **32,** 460–462 (2007); ibid. **32,** 1059 (2007)
23. M. D. Nielsen and N. A. Mortensen, "Photonic crystal fibers design based on the v-parameter," Opt. Lett. **11,** 2762–2764 (2003)
24. D. Grischkowsky, S. R. Keiding, M. van Exter, and Ch. Fattinger, "Far-infrared time-domain spectroscopy with terahertz beams of dielectrics and semiconductors," J. Opt. Soc. Am. B **7,** 2006–2015 (1990)
25. P. Uhd Jepsen, R. H. Jacobsen, and S. R. Keiding, "Generation and detection of terahertz pulse from bias semiconductor antennas," J. Opt. Soc. Am. B **13,** 2424–2436 (1996)
26. G. P. Agrawal, *Nonlinear Fiber Optics* (4th Edition), Academic Press (2007)
27. G. Zhao, R. N. Shouten, N. van der Valk, W. Th. Wenckebach, and P. C. M. Planken, "Design and performance of a THz emission and detection setup based on a semi-insulating GaAs emitter," Rev. Sci. Instrum. **73,** 1715–1719 (2002)
28. J. Toft Kristensen, A. Houmann, X. Liu, and D. Turchinovich, "Low-loss polarization-maintaining fusion splicing of single-mode fibers and hollow-core photonic crystal fibers, relevant for monolithic fiber laser pulse compression," Opt. Express **16,** 9986–9995 (2008)
29. Y. H. Lo and R. Leonhardt, "Aspheric lenses for terahertz imaging," Opt. Express **16,** 15991–15998 (2008)

1. Introduction

Electromagnetic radiation at terahertz (1 THz = 10^{12} Hz) frequencies interacts strongly with systems that have characteristic lifetimes in the picosecond range and/or energies in the meV range, and for that reason the THz range hosts a wealth of physical phenomena. The availability of broadband photonic components for the terahertz frequency range [1] has enabled studies of interaction between terahertz-frequency light and matter, and thus given unique insight into dynamics of complex biological [2] and solid-state systems [3] as well as fundamental electromagnetic phenomena [4]. Tightly confined guided propagation of THz fields allows strong interaction with small sample volumes, enabling development of new sensing applications.

The strong drive for exploration of the THz region has advanced the field of THz photonics significantly. Parallel to the impressive development of THz sources and detectors there has been significant development of new concepts for guided propagation of THz fields. Examples include dispersive propagation in square and circular metallic waveguides [10] and in plastic ribbon waveguides [11], dispersion-less propagation in parallel-plate waveguides [12], metallic ribbon waveguides [13], metallized glass tubes[16], and weakly guided THz wave propagation

#108854 - $15.00 USD Received 16 Mar 2009; revised 4 May 2009; accepted 4 May 2009; published 6 May 2009

on thin metallic wires [14] and in polymer wires[15].

Index-guiding photonic crystal fibers (PCFs) for the THz range with losses in the 0.5-2 dB/cm range have been demonstrated by stacking of polymer rods [17, 18]. The drill-and-draw technique used for the fabrication of the first microstructured polymer optical fibers[19] was later adapted for air-core Bragg fibers with appropriate dimensions for THz guidance, with a loss of 0.9-1.3 dB/cm over the 0.6 THz transmission bandwidth [20]. Simulations of air-core PBG fibers with triangular hole structure predict a loss in the range of 0.05 dB/cm in the narrow (0.1-0.2 THz) guiding region [21].

Hassani *et al.* [6, 7] and independently Atakaramains *et al.* [8, 9] recently proposed a novel guiding mechanism with high confinement of the guided mode in the core of an sub-wavelength diameter air-clad step-index fiber (a thin wire) with a distribution of sub-wavelength holes inside the wire. The field in such porous THz fibers is locally enhanced in the air holes. Hence a significant part of the field is located in air, leading to simulated losses in the range of 0.1-0.5 dB/cm, 1-2 dB/cm, and 0.1-0.2 dB/cm in teflon, polymethyl methacrylate (PMMA), and Topas® wires, respectively.

Here we report on fabrication and full optical characterization of a new class of broadband, single-mode photonic crystal fibers (PCFs) [5] designed for low-loss operation in the THz range with tailored dispersion and zero-dispersion frequencies near 0.6 THz. We show near-field images of the electric field amplitude and phase of the propagating mode in a photonic crystal fiber, visualizing single-mode propagation over a wide frequency range, the onset of higher-order mode propagation at high frequencies, and indication of the predicted porous guiding at low frequencies and high porosity [6, 7, 8, 9].

The amplitude- and phase-resolved imaging of the field profile is unrivalled at near-infrared and visible wavelengths, and thus characterization of fibers designed for THz frequencies is helpful not only for this specific type of specialty fiber, but for also for the general design of advanced optical fibers for any wavelength range.

We use the cyclic olefin copolymer Topas® to manufacture bendable THz fibers. We combine the low loss and low material dispersion of Topas® in the THz regime with a drill-and-draw technique [22] to fabricate a novel class of single-mode polymer THz PCFs, here exemplified with two fibers designed for low and high dispersion, respectively.

Given that our class of THz fibers confine the THz beam to the core with low loss over a broad transmission bandwidth, the fibers can be bent around tight corners, and can be mass-fabricated in long uniform fiber lengths, they represent a significant advancement in THz fiber technology.

2. Fabrication of THz fibers

We consider two fiber designs, both based on Topas® canes with an outer diameter of 6 mm, a large mode area (LMA) fiber and a small mode area (SMA) fiber. The LMA fiber has a pitch of 560 μm and a hole diameter of 250 μm, giving a hole diameter to pitch ratio of 0.45. The SMA fiber has a pitch of 350 μm and a hole diameter of 280 μm, giving a ratio of 0.8. The hole diameter to pitch ratio gives an indication of the mode characteristics of the fiber. A low hole to pitch ratio gives a single-mode fiber and a large ratio gives a multi-mode fiber [23]. At short wavelengths many modes may exist also for low-ratio fibers.

The fibers were manufactured using a drawing tower specially designed for the drawing of polymer optical fibers with diameters of 100-500 μm. An intermediate step in the drawing process is the drawing of a cane from the preform, which is then sleaved and drawn again. The cane is about 6 mm in diameter and the dimensions of the cane are therefore well suited for guiding THz frequencies.

The material used for the fibers was a cyclic olefin copolymer (COC) with the tradename

#108854 - $15.00 USD Received 16 Mar 2009; revised 4 May 2009; accepted 4 May 2009; published 6 May 2009

Topas® COC 8007, obtained from Topas Advanced Polymers, Inc. The COC granulates were cased into cylinders and then used as preforms. The desired photonic crystal hole structure was drilled into each polymer preform, and this structure was then preserved throughout the drawing process. The diameter of the preforms was 60 mm and the holes were 3 mm in diameter.

The bulk dielectric properties of Topas® were characterized by standard THz time-domain spectroscopy (THz-TDS, see Sec. 3) on a preform cylinder of 2 cm thickness. A similar sample of PMMA was also characterized. Figure 1 shows the attenuation and index of refraction of Topas® and PMMA.

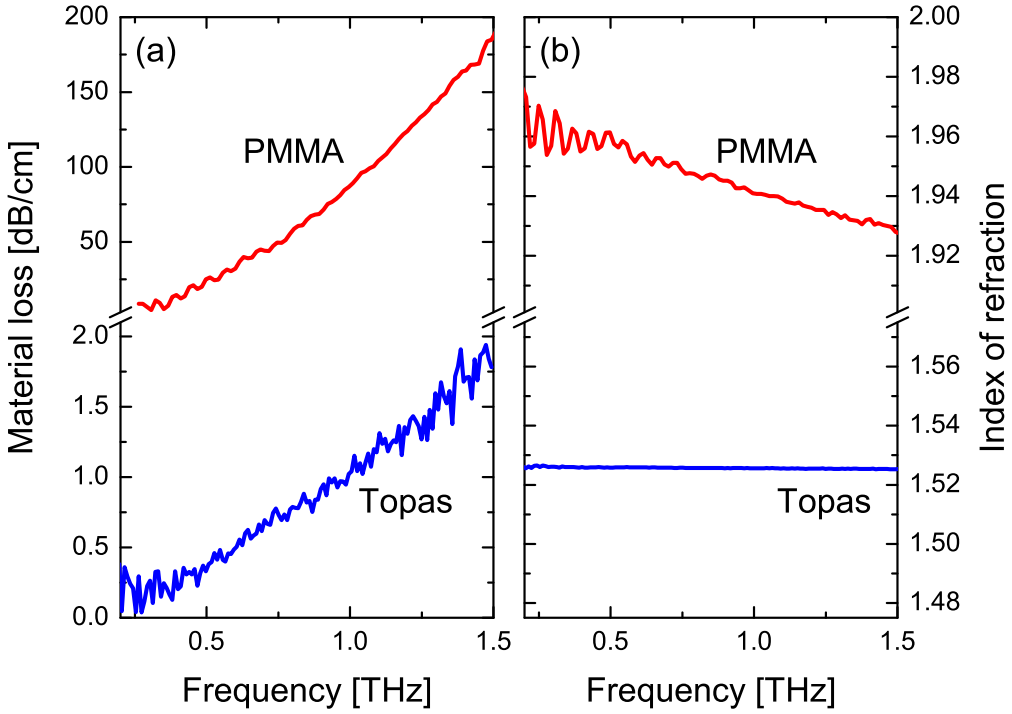

Fig. 1. (a) Material loss in the 0.2-1.6 THz range of bulk Topas and bulk PMMA. (b) Index of refraction in the 0.2-1.5 THz range of bulk Topas and bulk PMMA.

Due to the amorphous structure of the nonpolar COC, the bulk material loss of Topas® is approximately 100 times smaller than that of PMMA, and the index of refraction has a constant value of $n = 1.5258 \pm 2 \cdot 10^{-4}$ in the 0.1-1.5 THz range.

The drilled preform was placed in the draw tower and heated to above the glass transition temperature of the polymer using a convection oven. When the preform had softened it was pulled into canes of approximately 6 mm in diameter and lengths up to several meter. This cane constitutes the completed THz fiber. An optical fiber for shorter (near-IR) wavelengths can be fabricated in an additional draw step using the cane as starting material.

The completed THz fiber is a very robust and reproducible construction. The fabrication method guarantees high uniformity of the fiber cross section along the fiber length, low sensitivity towards external forces, and the possibility of straightforward postprocessing, such as fusion to other fibers, cutting, and tapering. Figure 2 shows photographs of cleaved facets of the LMA fiber and SMA fiber as well as fiber pieces shaped into 90-degree bends. The bending was performed after gentle heating of the completed THz fiber to a temperature above the glass

#108854 - $15.00 USD Received 16 Mar 2009; revised 4 May 2009; accepted 4 May 2009; published 6 May 2009

transition temperature. The integrity of the fiber was conserved during and after the bending process, and the hole structure was intact, judged by visual inspection.

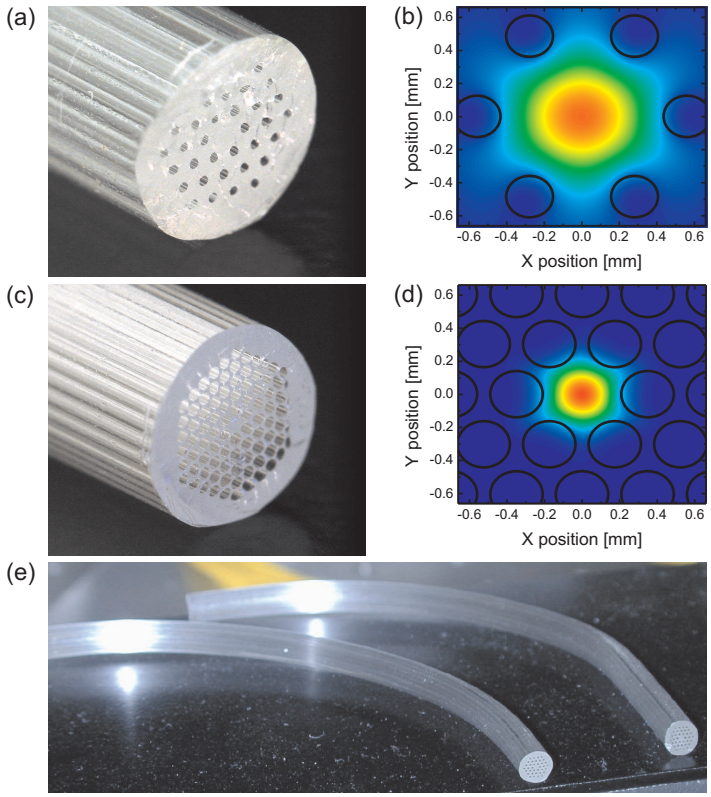

Fig. 2. (a) Photograph and (b) calculated fundamental guided mode structure at 1 THz of the large mode area (LMA) fiber, and (c) photograph and (d) calculated fundamental mode structure at 1 THz of the small mode area (SMA) fiber. (e) Photograph of LMA fibers shaped into 90° bends.

A contour plot of the spatial profiles of the electric field of the fundamental mode in the LMA and the SMA fibers at a frequency of 1 THz, calculated by the finite element method with the standard commercial software COMSOL, are shown together with the position of the air holes next the respective photographs of the fibers in Fig. 2. The effective area at 1 THz of the SMA mode and the LMA mode is 0.11 mm^2 and 1.86 mm^2, respectively, and hence the field is confined to the core region at 1 THz.

Both fibers were designed to be non-polarization maintaining, so in principle the state of the polarization of the THz light could change upon propagation. We have, however, taken care to work with fiber segments without twists of the hole structure along the fiber length. This is easily checked by visual inspection due to the macroscopic dimensions of the fibers and their transparency in the visible.

3. Experimental methods

For the transmission measurements we used a standard THz-TDS system[24, 25] driven by 100-fs laser pulses and using photoconductive switches for generation and detection of broadband

#108854 - $15.00 USD Received 16 Mar 2009; revised 4 May 2009; accepted 4 May 2009; published 6 May 2009

THz pulses. The collimated beam of single-cycle THz pulses were coupled in and out of the THz fibers with hyperhemispherical Topas® lenses with a diameter of 10 mm. Compared to a silicon hyperhemispherical lens ($n_{Si} = 3.4177$), the Topas® lens has a much lower refractive index. This results in lower reflection losses at the dielectric interfaces while keeping a good overlap between the free-space mode and the guided mode. Lo and Leonhardt [29] recently devised aspheric lens designs for THz applications which would further increase the coupling efficiency into the THz fibers.

The THz-TDS setup was modified to allow either transmission measurements of straight and bent lengths of fiber or reflection measurements at normal incidence for the cut-back loss measurements, in order to assure identical coupling and free-space imaging of the THz beam coupled in and out of the different fiber lengths. In the reflection configuration the THz signal was reflected at the back end facet of the fiber by a metallic reflector in close contact with the fiber facet, and hence it traversed the fiber length two times.

The modal structure of the THz field propagating through the fibers was measured directly at the end facet of the fiber using a near-field probe. The high spatial resolution required for the direct modal characterization was obtained by coupling of a freely propagating single-cycle, broadband THz pulse [27] onto one end facet of a piece of the fiber, and positioning the other facet of the fiber directly on a gallium phosphide electro-optic field sensor. This sensor measured the temporal profile of the transmitted THz field by ultrafast free-space electro-optic sampling using a tightly focused beam of femtosecond laser pulses, split off from the beam of pulses generating the THz pulses [4]. The spatial resolution was nominally 10 μm, determined by the focal spot size of the probe beam. This corresponds to a deep sub-wavelength resolution of $\lambda/300$ at 100 GHz, and $\lambda/30$ at 1 THz.

4. Characterization of loss and dispersion

In Figs. 3(a) and 3(b) we show the time traces and spectrograms of broadband THz pulses [24, 25] after propagation through 29 mm of LMA fiber and through 26 mm of SMA fiber, respectively. The spectrograms are calculated from the measured time traces of the electric field of the THz output pulses using a sliding Gaussian-shaped time window of 3 ps. The ringing of the field after the main pulse is caused by rotational transitions in the water vapor in the THz beam path atmosphere excited by the broadband THz pulse.

The dispersion parameter $\beta_2 = (1/2\pi c)(\nu\partial^2 n_{\text{eff}}/\partial\nu^2 + 2\partial n_{\text{eff}}/\partial\nu)$ [26] of the fundamental mode of the LMA and SMA fibers are shown in Figs. 3(c) and 3(d), respectively. The LMA fiber has a zero-dispersion-frequency (ZDF) at 0.55 THz, and a rather small waveguide dispersion. The much stronger waveguide dispersion of the SMA fiber shifts the zero-dispersion frequency (ZDF) upwards to 0.6 THz and increases the slope of the dispersion around the ZDF. A positive value of β_2 corresponds to normal dispersion. Direct comparison of the spectrograms and the dispersion curves in Fig. 3 confirms the predicted dispersion curves. Frequency components below the ZDF in the SMA fiber arrives several tens of picoseconds before frequency components at and above the ZDF. This effect is less pronounced in the LMA fiber but still clearly visible.

In order to measure the loss of the Topas® fiber, a cutback experiment was performed, where transmission measurements in a double-pass reflection geometry were carried out as indicated in Fig. 4(a) on LMA fiber lengths ranging from 3 mm to 46 mm, corresponding to propagation lengths from 6 mm to 92 mm. Using this geometry, we could assure that the free-space beam path of the THz spectrometer, as well as the coupling in and out of the fiber, was kept constant during the measurements on different lengths of the fiber.

The time traces in Fig. 4(b) represent THz pulses recorded after propagating the specified distances through the LMA fiber. The pulses have been time-shifted to peak at $t = 0$ ps and

#108854 - $15.00 USD Received 16 Mar 2009; revised 4 May 2009; accepted 4 May 2009; published 6 May 2009

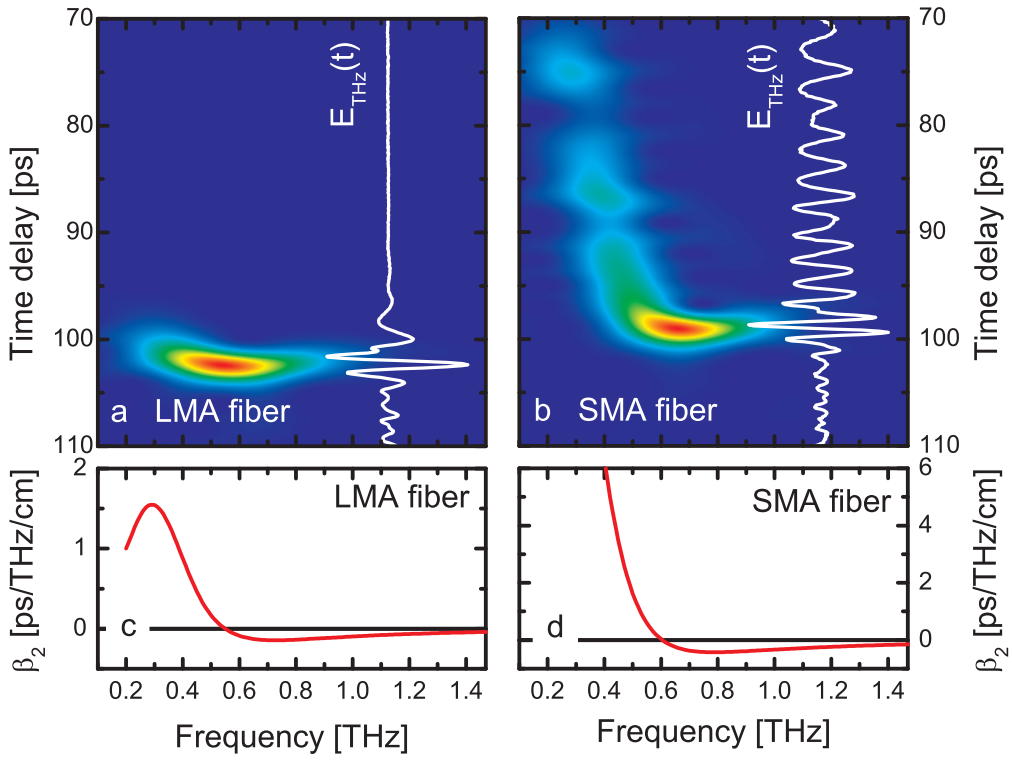

Fig. 3. Spectrogram and measured temporal profile of the THz pulse after propagation through (a) 29 mm LMA fiber and (b) 26 mm SMA fiber. The color scale is linear and shows the spectral amplitude of the THz field. Calculated dispersion parameter β_2 of (c) the LMA fiber and (d) the SMA fiber. Positive values of β_2 indicate normal dispersion, negative values indicate anomalous dispersion.

offset vertically for a clear representation.

The black squares in Fig. 4(c) show the attenuation $10\log(I/I_0)$ of the THz signal intensity ($I = \int E^2(t)dt$) as function of the LMA fiber length L. A linear fit to the experimental data shows an average loss of $\alpha_{\mathrm{dB}} = (0.4 \pm 0.08)$ dB/cm, or an average absorption coefficient of $\alpha = (0.09 \pm 0.02)\ \mathrm{cm}^{-1}$.

The black squares in Fig. 4(d) show a measurement of the frequency-dependent loss of the LMA fiber, obtained by analysis of the full spectra of the transmitted THz pulses at different propagation lengths. For comparison, the gray line shows the bulk loss of Topas®. At low frequencies the propagation loss increases steeply, most probably due to loss of confinement. At high frequencies the loss also increases due to a combination of increasing material loss and increased sensitivity towards scattering and microbend losses. Interestingly, the region between 0.4 and 0.6 THz displays a significantly lower propagation loss than in bulk Topas®. Several effects may contribute to this very low loss. Firstly, in spite of the confinement of the propagating mode to the solid core of the fiber, a significant portion of the field still propagates in the lossless air regions near the core, and hence an effective loss lower than the bulk value can be observed. Secondly, we expect scattering losses due to interface roughness in the airhole structure of the drawn fiber to be negligible due to the long wavelength of the light and the smooth appearance of the airholes. Thirdly, we note that the bulk loss measurement was carried out on

#108854 - $15.00 USD Received 16 Mar 2009; revised 4 May 2009; accepted 4 May 2009; published 6 May 2009

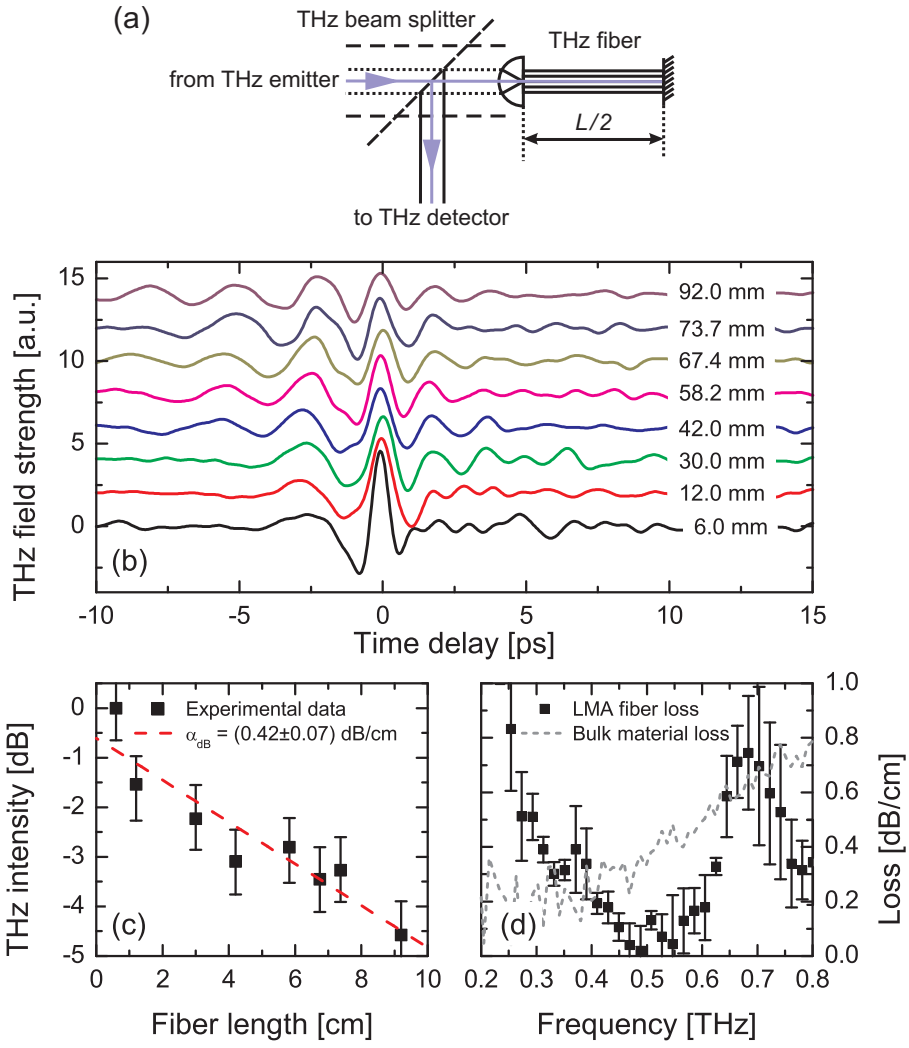

Fig. 4. (a) Reflection THz-TDS geometry for constant in- and outcoupling of the THz signal during loss measurements. (b) Time traces of THz pulses propagated through the specified distance in the LMA fiber. Pulses have been shifted in time and offset vertically for clarity. (c) Time-averaged loss of the LMA fiber (solid square symbols). The error bars are conservative estimates of the standard deviation, based on two subsequent measurements of the same length of fiber after removing and re-inserting the fiber segment in the experimental setup. The inset shows the experimental configuration for the cutback measurement and the full line shows a linear fit to the experimental data. (d) Frequency-resolved loss curve (square symbols) compared to the bulk loss in Topas® (gray line). The error bars show the standard deviation between three measurements on different fiber lengths.

#108854 - $15.00 USD Received 16 Mar 2009; revised 4 May 2009; accepted 4 May 2009; published 6 May 2009

a segment of a preform. The effect of the draw process on the optical properties of Topas in the THz range has not yet been investigated.

5. Measurement of modal profiles

The modal structure of the THz field propagating through the fibers was measured directly at the end facet of the fiber using a near-field probe [27, 4]. Figures 5(a) and 5(b) show the measured electric field distribution on a linear scale in the central region of the LMA fiber at 0.2 THz and at 1.0 THz, normalized to the peak of the electric field at the center of the distribution. Figures 5(c) and 5(d) show the corresponding field distribution in the SMA fiber.

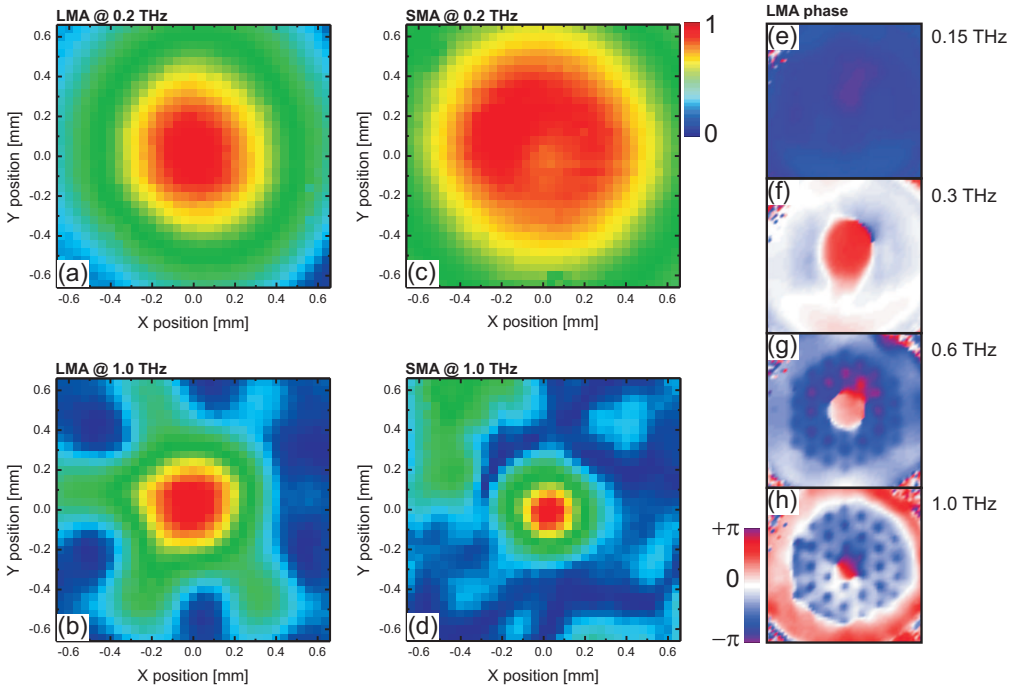

Fig. 5. Measured modal structure of the electric field of the propagating mode through the LMA fiber at (a) 0.2 THz and (b) 1.0 THz, and through the SMA fiber at (c) 0.2 THz and (d) 1.0 THz. Panels (e)-(h) show the phase of the frequencies 0.15, 0.3, 0.6, and 1.0 THz across the LMA fiber facet.

At 1.0 THz the field is significantly more concentrated in the SMA fiber than in the LMA fiber, as expected from the modal calculations shown in Fig. 2. In general the agreement between the simulated and measured mode profiles is good. Note that the orientation of the fibers in Fig. 5 is rotated 30° with respect to the modal profiles in Fig. 2.

At 0.2 THz, on the other hand, the confinement of the mode is stronger in the LMA fiber than in the SMA fiber. We believe that the larger mode area at 0.2 THz in the SMA fiber is the experimental observation of the onset of guided propagation in a microporous environment, as predicted by simulations by Hassani *et al.* [6, 7] and Atakaramians *et al.* [8, 9]. At 0.2 THz (1500 μm wavelength) the hole diameter of 250 μm is 6 times smaller than the wavelength. The porosity of the SMA fiber is 28% [8], and hence the SMA fiber cross section becomes similar to a microporous environment. This similarity breaks down in the LMA fiber with its smaller porosity of 8%, and also at higher frequencies in both fiber types. In these situations

#108854 - $15.00 USD Received 16 Mar 2009; revised 4 May 2009; accepted 4 May 2009; published 6 May 2009

the solid core of the photonic crystal structure acts as the guiding element, as evident from Fig. 5.

We observe a smooth, Gaussian-shaped intensity profile of the mode profile in the SMA fiber at 0.2 THz, in contrast to the predicted field enhancement in the air regions in a microporous environment. The small, but finite air gap between the fiber end facet and the electro-optic sampling crystal, caused by slight imperfections in the cleaving process, will lead to spatial smearing of the measured near-field distribution. The evolution of the near-field, even over a few tens of microns away from the fiber facet, may mask the extremely localized regions of field enhancement.

The stray light observed in the image of the SMA mode at 1 THz is likely due to a combination of scattering due to imperfect cleaving of the fiber and the way the spatial recording was carried out, as described in the Methods section. The large air filling fraction leaves the SMA fiber facets rather sensitive to the cleaving method, and small fragments of polymer easily clog some of the air holes after cleaving, an effect also seen in photonic crystal fibers in the near-infrared range [28].

Figures 5(e) - 5(h) show the measured distribution of the phase of the THz signal propagated through the LMA fiber at frequencies ranging from 0.15 to 1.0 THz. At the lowest frequency we observe a constant phase across the whole fiber cross section, indicating that the fiber as a whole is responsible for the guiding. This we again interpret as an indicator of the onset of propagation in a microporous environment.

At higher frequencies the signal in the core region of the fiber is out of phase with the signal in the cladding region of the fiber. This is a direct consequence of guiding in the fundamental mode in the solid core of the fiber. Interestingly, at the highest frequencies we observe an onset of higher-order propagation in the solid core, seen as a phase shift across the core region. The insight into the guiding properties of the fibers offered by the amplitude and phase resolved near-field THz imaging is unique, and the data in Fig. 5 is unrivaled by current technology for characterization of optical fibers in the near-IR.

Due to the scalability of dielectric fiber designs our results obtained on photonic crystal fibers in the THz region are directly transferable to other spectral regions and hence both THz transmission measurements and THz near-field imaging are versatile tools for general design of advanced photonic crystal fibers.

The drill-and-draw fabrication process enables highly uniform optical fibers for the THz frequency range to be manufactured with the full range of functionalities that we see today in applications of photonic crystal fibers in the near infrared. The robustness of the fibers during subsequent processing will pave the road to functional THz fiber based devices, such as couplers, Mach-Zehnder interferometers and fiber sensors, tapered fibers for field confinement and advanced dispersion management.

Acknowledgments

The EU TeraNova Program (RCN 71835) and the Lundbeck Foundation (Grant No. 170/06) are acknowledged for financial support of this work.

#108854 - $15.00 USD Received 16 Mar 2009; revised 4 May 2009; accepted 4 May 2009; published 6 May 2009